The Role of El Niño Southern Oscillation in driving Coastal Hazards in the U.S. Pacific Northwest

Meredith Leung*[1], Peter Ruggiero[1], Laura Cagigal[2], Dylan Anderson[3], Fernando Mendez[2]

[1]College of Earth, Ocean, and Atmospheric Sciences, Oregon State University, Corvallis, OR, USA
[2]Departamento Ciencias y Tecnicas del Agua y del Medio Ambiente, Universidad de Cantabria, Santander, Spain
[3]Coastal Hydraulics Laboratory, U.S. Army Engineer Research and Development Center, Duck, NC, USA

Supplementary Information

1) Methods

a) Annual Weather Type Construction

Annual Weather Types (AWTs) are constructed through a multi-step process following the methodology of Anderson et al. (2019) that begins with the extraction of monthly sea surface temperature anomalies (SSTAs) from the Nino3.4 bounding box. Hovmöller diagrams are constructed by taking the longitudinal average of SSTAs within the bounding box for each month of a boreal year (June to May). Empirical Orthogonal Function (EOF) analysis is applied to the Hovmöller diagrams, extracting dominant spatial modes and temporal behavior of observed ENSO dynamics. The three leading principal components (PCs) of the EOF analysis are clustered into six types (using K-means clustering) associated with canonical ENSO patterns (EP El Niño, CP El Niño, three transition/ neutral phases, and La Niña).

This custom ENSO index preserves orthogonal modes of variability that are critical for representing ENSO diversity and complexity (Almar et al., 2023; Williams and Patricola, 2018). The leading EOF captures the dominant seesaw of interannual SSTA variability represented by traditional ENSO indices (R^2>0.9 for both the ONI and Nino3.4 indices), while the second and third EOFs depict spatial and temporal patterns linked to shifting seasonal anomalies, and Kelvin wave propagation of SSTAs across the Pacific Basin, respectively (Anderson et al., 2019). By capturing more variance than classical ENSO indices (+19% compared to those that rely only on the leading EOF), this methodology is better able to represent the diversity of ENSO behavior on sub-seasonal to interannual scales.

b) Copulas

Multivariate gaussian copulas are used to define the joint probabilities between observed environmental parameters, maintaining realistic relationships between parameters while allowing for extrapolation of extremes (Cagigal et al., 2020; Anderson et al., 2019). Copulas are employed twice in the stochastic climate emulator methodology: in the simulation of new AWT principal components (PCs - representing ENSO behavior) and in the generation of synthetic hydrodynamic data (e.g., waves characteristics and storm surge).

Each copula is associated with a particular weather type (either an AWT or a DWT), and within each copula, every variable is fit to an appropriate marginal distribution (e.g., generalized extreme value, empirical, etc.). The marginal functions are transformed into a uniform distribution to estimate their joint dependence structures in gaussian space (Cagigal et al., 2020). In the case

of the 6 AWTs, a tri-variate gaussian copula is constructed using the marginal functions of the three leading AWT PCs. After synthetic chronologies of AWTs (timeseries of categories 1-6) are generated, AWT PCs are randomly sampled from the relevant gaussian copula to represent new sea surface temperature anomaly behavior, essentially ENSO events that are statistically plausible but not replicas of historical events.

The wave and storm surge copulas are constructed for each DWT. In these copulas observed wave heights, periods, and storm surge data are primarily fit to a GEV distribution, while wave direction is defined by an empirical fit. There are a few DWTs in which the wave period is strongly bi-modal, so an empirical fit applied. By using GEVs as the marginal distribution for most of the data, the probability of extreme events is better estimated than with other types of distributions (e.g., normal or empirical).

Wave parameters and storm surge are sampled for the peaks of wave hydrographs, which are parameterized from observed sea-state relationships to represent maximum flooding potential (Anderson et al., 2019). Wave height evolves hourly, following the hydrograph ramp up to and ramp down from peak flood potential, while other variables remain static for the hydrograph duration. This process of extrapolating from the peaks of hydrographs to hourly conditions can introduce some negative bias, particularly in the means of the wave height distributions. A bias correction is applied (Leung et al., 2024a) to address this, however exploring alternative methods of simulating the hydrodynamic variables at hourly timescale to avoid these biases is an important avenue of future research.

c) Auto-Logistic Regression Model

Synthetic sequences of weather types are generated via an auto-logistic regression (ALR) model. Auto-logistic regression enables simulation of categorical variables with non-normal distributions based on multiple covariates (Guanche et al., 2014). The ALR model is implemented in the stochastic climate emulator following the methodology presented in Anderson et al. (2019). The probability of a single weather type occurring for the given time period (e.g., year, day) can be represented with the inclusion of relevant covariates:

$$\text{Prob}(Y_t = i \mid Y_{t-1}, \dots, Y_{t-e}, X)_t = \frac{\exp\left(\pi_i^S + \pi_i^C + \pi_i^{AR}\right)}{\sum_{k=1}^{n_{WT}} \exp\left(\pi_k^S + \pi_k^C + \pi_k^{AR}\right)}$$

where seasonality is represented by:
$\pi_i^S = \beta_{0,i} + \beta_{1,i}\cos(\omega t) + \beta_{1,i}\sin(\omega t)$;

the influence of different weather type covariates are included via:
$\pi_i^C = \sum_{i=1}^{n_C} X_i \beta_i^C$;

and the influence of previous weather type states is introduced via a Markov chain, parameterized as:

$$\pi_i^{AR} = \sum_{j=1}^{d} Y_{t-j}\gamma_j$$

For daily weather type (DWT) simulation, covariates include seasonality, the three leading annual weather type PCs, two intraseasonal weather type (IWT) PCs, and a Markov chain accounting for *d* previous daily weather type states.

2) Results

a) Spatial Variability of ENSO-hydrodynamic teleconnections in the Pacific Northwest

The influence ENSO has on coastal hazard and hydrodynamic conditions is highly variable at global to regional scale (e.g., Vos et al., 2023; Aramburo et al., 2022). However, even within regions there can be significant variability due to complex interactions with local-scale processes and distinct behaviors caused by diverse ENSO events (e.g., Bromirski et al., 2005; Barnard et al., 2015). Comparisons of winter hydrodynamic anomalies conditioned on ENSO phase and strength can highlight sub-regional variability of ENSO teleconnections in the PNW (figure 4a & SI figure 1). While wave energy flux, water level, and wave directionality trends associated with ENSO phase and strength are consistent across the PNW, there is notable spatial variability within the region. At all three PNW sub-sites explored in figure 4a (Northern Oregon/Southern WA) and SI figure 1 (Northern WA and Northern CA), El Niño is associated with higher wave energy flux, water levels, and more southerly wave directionality. This trend is similarly shown for El Niño strength, while the opposite trend is seen for La Niña strength. However, across the three sub-sites the tails of the distributions are slightly different, as is the behavior of individual ENSO events. For example, all three hydrodynamic variables explored generally had longer tails at the more northerly sites, indicating larger ENSO-driven hydrodynamic extremes (both high and low) may be possible in Northern WA compared to Northern CA. Individual ENSO events can also be associated with very different hydrodynamic signals within the region. This can be seen in SI figure 1 through comparisons of the 1982-83 and 2015-16 El Niño events. In Northern WA, the 1982-83 and 2015-16 El Niño events generated roughly equal winter wave energy flux anomalies (~42 W/m). However, in Northern CA, the 2015-16 event was approximately 10 W/m less energetic than the 1982-83 event. While both locations saw similar water level anomalies during the two ENSO events, wave direction approached from a much more southerly angle in Northern WA (~ -5° to -10°) compared to Northern CA (~ -1° to -8°). This comparison highlights that there is perceptible spatial variability in ENSO-coastal hazard teleconnections in the PNW, both in the overall probability distributions and when examining individual events.

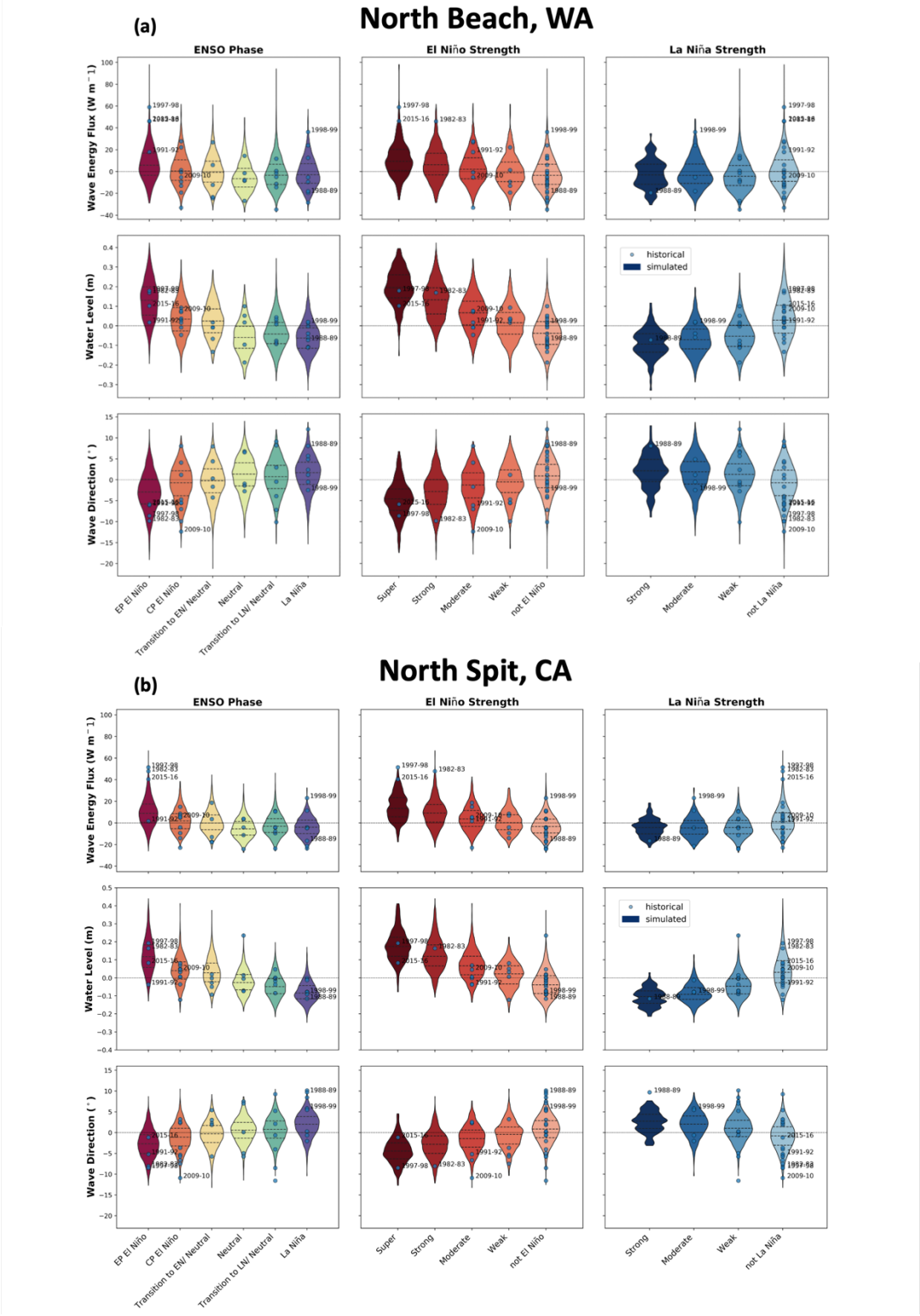

SI Figure 1. Mean winter (DJF) anomalies of wave energy flux (function of period and height), water level (storm surge + MMSL), and wave direction highlighting the alongshore variability of ENSO teleconnections. Anomalies are shown for (a) Northern Washington and (b) Northern California as compared to figure 4a. in the main text which shows Northern Oregon/ Southern Washington.

3) References

Almar, R., Boucharel, J., Graffin, M., Abessolo, G. O., Thoumyre, G., Papa, F., Ranasinghe, R., Montano, J., Bergsma, E. W. J., Baba, M. W., & Jin, F.-F. (2023). Influence of El Niño on the variability of global shoreline position. Nature Communications, 14(1), 3133. https://doi.org/10.1038/s41467-023-38742-9

Anderson, D., Rueda, A., Cagigal, L., Antolinez, J. A. A., Mendez, F. J., & Ruggiero, P. (2019). Time-Varying Emulator for Short and Long-Term Analysis of Coastal Flood Hazard Potential. Journal of Geophysical Research: Oceans, 124(12), 9209-9234. https://doi.org/10.1029/2019jc015312

Aramburo, D., Montoya, R. D., & Osorio, A. F. (2022). Impact of the ENSO phenomenon on wave variability in the Pacific Ocean for wind sea and swell waves. *Dynamics of Atmospheres and Oceans*, *100*, 101328. https://doi.org/10.1016/j.dynatmoce.2022.101328

Barnard, P. L., Short, A. D., Harley, M. D., Splinter, K. D., Vitousek, S., Turner, I. L., . . . Heathfield, D. K. (2015). Coastal vulnerability across the Pacific dominated by El Niño/Southern Oscillation. Nature Geoscience, 8(10), 801-807. https://doi.org/10.1038/ngeo2539

Bromirski, P. D., Cayan, D. R., & Flick, R. E. (2005). Wave spectral energy variability in the northeast Pacific. Journal of Geophysical Research: Oceans, 110(C3). https://doi.org/10.1029/2004JC002398

Cagigal, L., Rueda, A., Anderson, D., Ruggiero, P., Merrifield, M. A., Montaño, J., . . . Méndez, F. J. (2020). A multivariate, stochastic, climate-based wave emulator for shoreline change modelling. Ocean Modelling, 154. https://doi.org/10.1016/j.ocemod.2020.101695

Guanche, Y., Mínguez, R., & Méndez, F. J. (2013). Autoregressive logistic regression applied to atmospheric circulation patterns. *Climate Dynamics*, *42*(1–2), 537–552. https://doi.org/10.1007/s00382-013-1690-3

Vos, K., Harley, M. D., Turner, I. L., & Splinter, K. D. (2023). Pacific shoreline erosion and accretion patterns controlled by El Niño/Southern Oscillation. Nature Geoscience, 16(2), 140-146. https://doi.org/10.1038/s41561-022-01117-8

Williams, I. N., & Patricola, C. M. (2018). Diversity of ENSO Events Unified by Convective Threshold Sea Surface Temperature: A Nonlinear ENSO Index. Geophysical Research Letters, 45(17), 9236–9244. https://doi.org/10.1029/2018GL079203